

# Experiment and Large-Eddy Simulation on Free Air Jets Issuing from a Rectangular Nozzle with Deflectors

Riku Ouchi<sup>1,2\*</sup>, Takahiro Kiwata<sup>3</sup>, Naoki Kajitani<sup>1</sup>, Hiroshi Teramoto<sup>4</sup>

<sup>1</sup>Graduate School of Natural Science and Technology, Kanazawa University, Ishikawa, Japan

<sup>2</sup>Thermal Management Systems R&D Div., DENSO CORP, Aichi, Japan

<sup>3</sup>School of Mechanical Engineering, Kanazawa University, Ishikawa, Japan

<sup>4</sup>Department of Mechanical Engineering, National Institute of Technology, Ishikawa College, Ishikawa, Japan

Email: \*rikuouchi@stu.kanazawa-u.ac.jp

**How to cite this paper:** Ouchi, R., Kiwata, T., Kajitani, N. and Teramoto, H. (2021) Experiment and Large-Eddy Simulation on Free Air Jets Issuing from a Rectangular Nozzle with Deflectors. *Journal of Flow Control, Measurement & Visualization*, 9, 73-92.

<https://doi.org/10.4236/jfcmv.2021.94005>

**Received:** July 15, 2021

**Accepted:** October 22, 2021

**Published:** October 25, 2021

Copyright © 2021 by author(s) and Scientific Research Publishing Inc. This work is licensed under the Creative Commons Attribution International License (CC BY 4.0).

<http://creativecommons.org/licenses/by/4.0/>



Open Access

## Abstract

The purpose of the present study was to establish a passive flow control method for a rectangular jet using two types of deflectors installed symmetrically inside a nozzle. This deflector in a rectangular nozzle generates the rectangular coaxial jets. The effect of the slant angle of the deflectors on the flow characteristics and the spread of the rectangular jet was investigated experimentally and by large-eddy simulation. The experiment and the numerical simulation were carried out at a Reynolds number of 9000. The rectangular jet with no deflectors generates a vortex ring from the nozzle exit. The vortex ring collapses in the downstream region and the outline of the jet changes from rectangular to diamond-shaped as a result of the axis-switching phenomenon. The rectangular jet with divergent and convergent deflectors shows particularly noticeable changes in the flow characteristics and vortical structures, as compared to the case with no deflectors. In the case of the rectangular jet with divergent deflectors (slant angle of  $\alpha = 6^\circ$ ), minor axis spread is promoted more than major axis spread, and axis switching occurs closer to the nozzle exit than that in the case of no deflectors. The outline of the jet also changes from lateral rectangular to vertical rectangular as a result of axis switching. On the other hand, in the case of a rectangular jet with convergent deflectors ( $\alpha = -6^\circ$ ), minor axis spread is suppressed more than major axis spread, and axis switching occurs farther from the nozzle exit than that in the case with no deflectors. The outline of the jet does not change until the downstream region. Therefore, the spread and the axis-switching location for the rectangular jet can be controlled by the deflectors inside the rectangular nozzle.

---

## Keywords

Jet, Rectangular Nozzle, Deflectors, Flow Control, Flow Measurement, Numerical Simulation, LES

---

## 1. Introduction

Having a good understanding of vortical structures in free shear layers such as jets is important for the control of aerodynamic noise and the enhancement or suppression of flow mixing. Methods of enhancing and suppressing mixing in jet flows have been studied for the past half-century. Numerous studies on jets issuing from a non-circular nozzle have been conducted [1]-[11]. Particularly, triangular [3], square [4], rectangular [5] [6], and elliptical [7] jets can improve the mixing performance in the flow field.

Rectangular jets essentially combine the effects of the aspect ratio observed in elliptic jets and the corners observed in square jets. The flow structure in the rectangular jet contains streamwise vortices produced by secondary flow at the corner of the nozzle. The deformation of the rectangular vortex ring persists downstream and plays an important role in the spreading of this type of jet. Sfier [5] examined jets issuing from rectangular slots with different geometries and aspect ratios. It was found that the nozzle geometry plays a very important role in determining the rectangular jet development through the three-dimensional effects of the flow, and, in comparison to orifice jets, the flow emitted from the rectangular channel has a two-dimensional region that extends further downstream. Quinn [6] studied the influence of the aspect ratio on the turbulent free jet flow issuing from sharp-edged rectangular slots. His results demonstrate that the near-field mixing in the rectangular jet increases with increasing slot aspect ratio. In the case of an aspect ratio of 20, the jet had the shortest potential core and the highest shear-layer values of the turbulence kinetic energy and the Reynolds stress.

The effects on a jet of notches, grooves, tabs, and deflectors placed in the near nozzle exit have also been studied. Fujita *et al.* [8] measured the potential core length, velocity decay, and half-velocity width of a 12.5:1 rectangular jet with rectangular notches. It was revealed that the potential core length takes a maximum value in the case of a notch aspect ratio of 12.5, causing a large secondary flow toward the jet centerline in the upstream region. Kumar *et al.* [9] conducted experiments on jets from a 2:1 rectangular nozzle with and without grooves. They demonstrated that the grooves do not significantly influence the overall jet mixing characteristics but considerably influence the axis-switching phenomenon. Verma *et al.* [10] experimentally studied a jet issuing from an elliptic nozzle with two cylindrical tabs at a Reynolds number of  $5.08 \times 10^4$ . Increasing the tab height shifted the location of the end of the jet potential core further upstream and promoted higher jet half-width growth along the plane of the major axis. As

a result, axis switching in the tabbed elliptic jet was not observed. Hinomoto *et al.* [11] examined the effect of deflectors installed symmetrically inside an 8.8:1 rectangular nozzle on the flow characteristics of the elongated rectangular jet with the side walls. It was found that the spread of a plane jet with divergent deflectors is larger than that of a jet with no deflectors. However, the spread of a plane jet with convergent deflectors is smaller than those of jets with divergent deflectors and without deflectors.

However, it is unknown that the deflectors inside the rectangular nozzle with a low aspect ratio are effective to control the spread of a rectangular jet which has the three-dimensional flow structures such as the axis-switching phenomenon. Thus, the purpose of this study is to establish eventually a passive flow control method for the spread of a rectangular jet with  $AR = 2.17$  using deflectors installed symmetrically inside a nozzle. This aspect ratio was determined by referring to the dimensions of the nozzle of a car air conditioner. The present paper was investigated using two-component hot-wire anemometer measurements and three-dimensional numerical simulation by the large-eddy simulation (LES). Our final goal is to make the small spread rectangular jet.

## 2. Experimental Apparatus and Techniques

### 2.1. Experimental Setup

**Figure 1** shows a schematic diagram of the experimental apparatus. Velocity measurement and flow visualization were carried out using a blow-down wind tunnel. An axial fan was used to supply airflow to the rectangular nozzle. The rectangular nozzle had a double contraction with dimension reduction ratios of 3.3:1 and 2.8:1. **Figure 2** shows three-dimensional diagrams and cross-sections of rectangular nozzles with parallel plates and deflectors. The rectangular nozzle had a height  $H$  of 30 mm, a width  $B$  of 65 mm, and a length of 100 mm. The thickness of the deflector plate  $t$  was 0.8 mm. The angles between the parallel plates, the divergent deflector plates, and the convergent deflector plates were  $\alpha =$

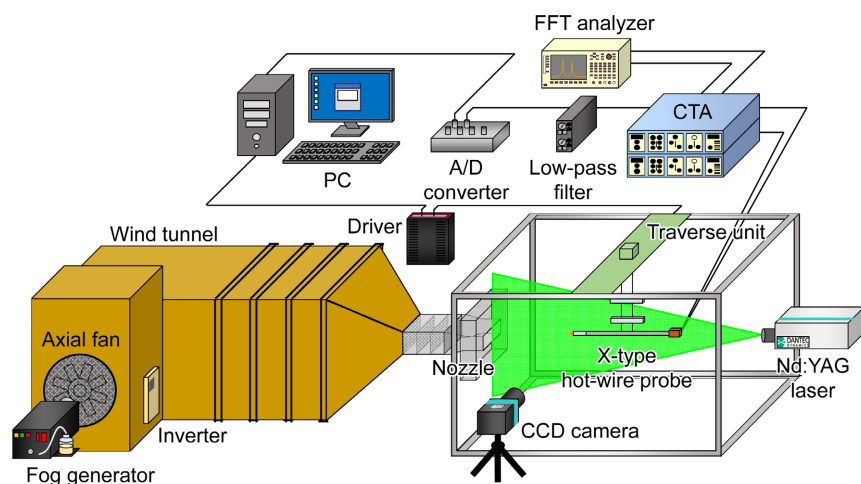


**Figure 1.** Schematic of the experimental apparatus.

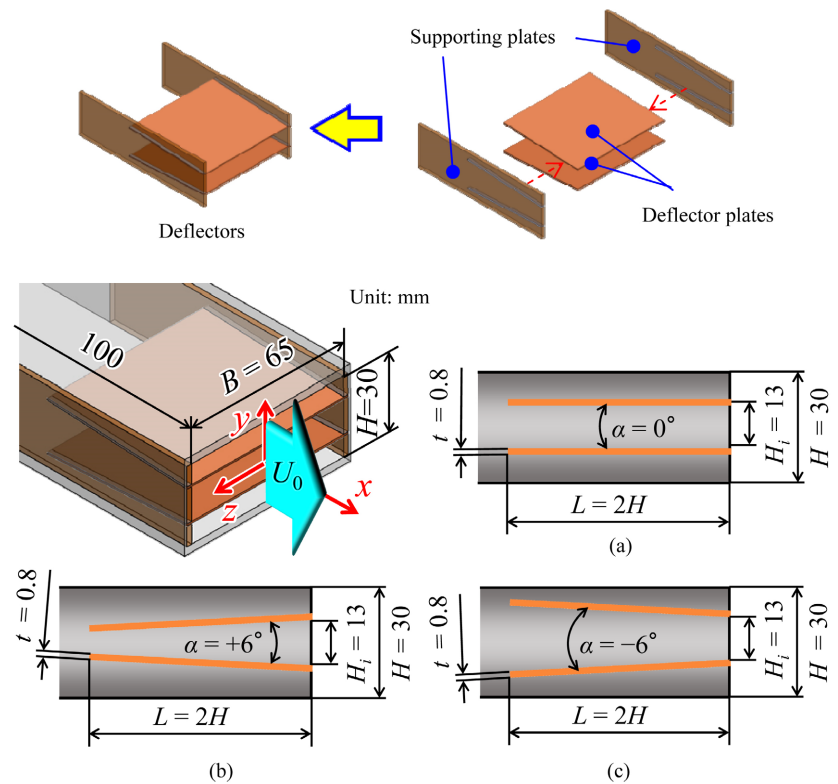


**Figure 2.** Schematic diagram of the rectangular nozzle with deflectors and the cross-section of nozzles. (a) Parallel plates; (b) Divergent deflectors; (c) Convergent deflectors.

$0^\circ$ ,  $6^\circ$ , and  $-6^\circ$ , respectively. The mean and fluctuating velocities were measured using an X-type hot-wire probe and a constant-temperature hot-wire anemometer with a linearized output. The output signals of the hot-wire probe were converted by a 12-bit analog-to-digital (A/D) converter with a sampling frequency of 10 kHz, and  $10^5$  data points were stored. A computer-controlled traversing mechanism was used for probe positioning. Experiments were performed under computer control for automated data acquisition. The mean velocity and turbulence intensity were obtained using a personal computer. The velocity profile for the rectangular jet at the nozzle exit exhibited a flat-topped shape. The mean bulk velocity  $U_0$  and the turbulence intensity  $u'_{rms}/U_0$  at  $x/H = 0.1$  from the nozzle exit were 4.5 m/s and 0.7%, respectively. This wind speed corresponds to the low level of a car air conditioner. The Reynolds number  $Re_H (= U_0 H / \nu$ , where  $\nu$  is the kinematic viscosity of air) was approximately 9000.

Flow visualization was carried out under the same conditions as the flow measurement experiments. To visualize the flow, an oil mist was injected into the wind tunnel. A pulsed Nd:YAG laser was used to visualize vortical structures, and images were recorded by a CCD camera.

## 2.2. Computational Techniques

Three-dimensional numerical simulations were performed using the large-eddy simulation (LES) of the commercial computational fluid dynamics (CFD) soft-

were ANSYS Fluent 17.2 to investigate the flow structures of a rectangular jet by solving the unsteady Navier-Stokes and continuity equations. Calculations were carried out at  $Re = 9000$ . The flow field was assumed to be unsteady, viscous, and incompressible. The working fluid was air ( $15^\circ\text{C}$ ) with a density of  $1.225 \text{ kg/m}^3$  and a viscosity of  $1.7894 \times 10^{-3} \text{ Pa}\cdot\text{s}$ . The pressure implicit with splitting of operator (PISO) method was used as the calculation algorithm for the pressure-velocity coupling. The convection terms in the governing equation were discretized by the bounded central differencing scheme. Second-order central differencing was used for the diffusion term, whereas the second-order implicit scheme was used for the time marching.

The computational domain, mesh, and boundary conditions are shown in **Figure 3**. The streamwise and transverse lengths of the computational domain were set to  $600 \text{ mm}$  ( $=20H$ ) and  $450 \text{ mm}$  ( $=15H$ ), respectively. The nozzle geometry was defined to correspond to the experimental setup ( $H = 30 \text{ mm}$ ,  $B = 65 \text{ mm}$ ). Since the boundary layer in the deflectors occurs the flow separation on the walls easily and turbulence models must be quite sensitive in the vicinity of the mesh spacing near the wall and nozzle to yield accurate predictions, the computational meshes used for the LES were set finer than those for the laminar simulations. Therefore, the minimum cell size is  $0.1 \text{ mm}$  near the walls. The numbers of grid point in the  $x$ ,  $y$ , and  $z$  directions were 231, 222, and 251, respectively. A total of approximately  $1.1 \times 10^7$  grid points were nonuniformly distributed in the computational domain. The Courant number is less than 0.1.

A uniform velocity profile corresponding to the nozzle exit velocity was specified at the inlet boundary. The velocity on the upper and lower inlet surfaces, which were outside of the rectangular nozzle inlet surface, was adjusted to  $0.03 U_0$  to maintain a weak straight flow aligned toward the entrainment flow outlet [12]. The nonslip boundary condition was applied to the walls of the rectangular nozzle. The slip condition was applied at the periphery of the computational domain, where the gradients of all variables were set to be equal to zero. A pressure outlet condition of  $p = 0$  was specified at the downstream boundary of the domain.

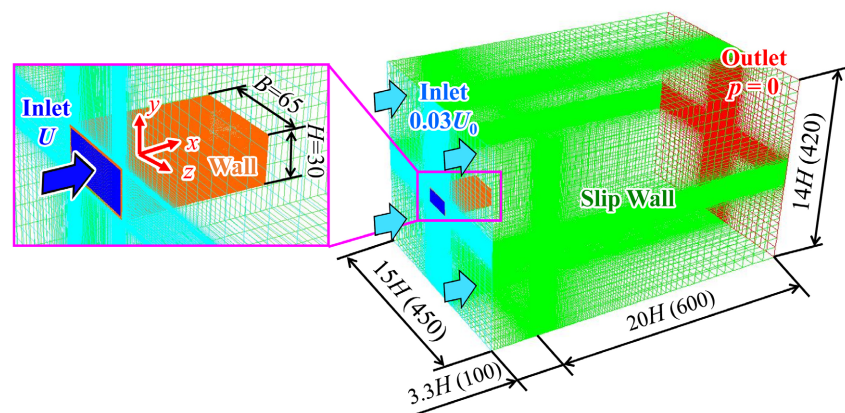


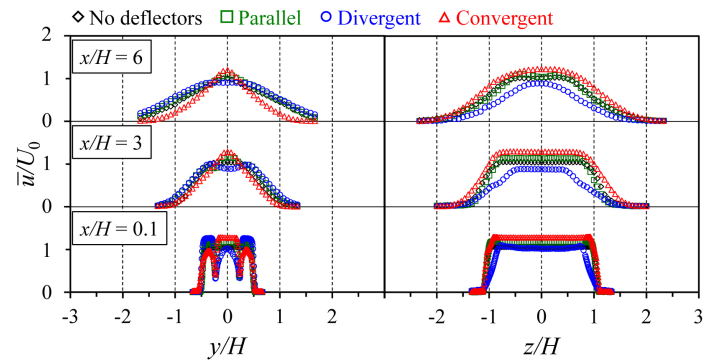
**Figure 3.** Computational domain, mesh, and boundary conditions.

### 3. Results and Discussion

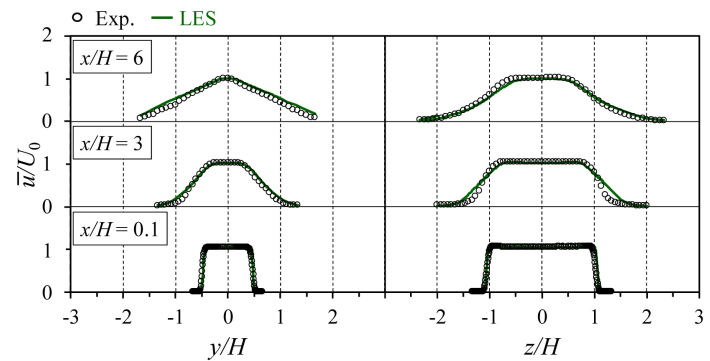
#### 3.1. Mean Velocity and Turbulence Intensity in the $x$ - $y$ and $x$ - $z$ Cross Sections

**Figure 4(a)** shows the profiles of the mean streamwise velocity  $\bar{u}/U_0$  in the  $x$ - $y$  plane along the minor axis at  $z = 0$ , and the  $x$ - $z$  plane along the major axis side at  $y = 0$  to compare the four jets, *i.e.*, nozzles with no deflectors, parallel plates, divergent deflectors, or convergent deflectors. The streamwise velocities were normalized with respect to the mean bulk velocity  $U_0$ . With respect to the velocity distribution at  $x/H = 0.1$  separated by deflectors, the jet on the central axis side is referred to as the inner jet, and the jets on both sides of the inner jet are referred to as the outer jets. The velocity profiles of the jets show good symmetry, in contrast with the central axis. For the jet with parallel plates, a velocity depression occurs between the inner and outer jets due to the wake of the parallel plates at  $x/H = 0.1$ . However, the ratio of the maximum velocity of the inner jet  $\bar{u}_{imax}$  to the outer jets  $\bar{u}_{omax}$  is  $\bar{u}_{imax}/\bar{u}_{omax} = 1.0$ , namely, each maximum velocity is approximately the same, since the angle between the parallel plates is  $0^\circ$ . For the jet with divergent deflectors, the velocity profile at  $x/H = 0.1$  exhibits a concave shape, and the velocity ratio is  $\bar{u}_{imax}/\bar{u}_{omax} = 0.8$ . Further downstream at  $x/H = 6$ , the concave shape disappears as the jet takes on a fully developed profile. In addition, the jet spread is larger than that of the other three jets. For the jet with convergent deflectors, the velocity ratio is  $\bar{u}_{imax}/\bar{u}_{omax} = 1.3$ . The velocity profile has a convex shape at  $x/H = 0.1$ , that is, the velocity of the inner jet is larger than that of the outer jets. The jet spread at  $x/H \geq 3$  is smaller than that of the other three jets. It can be seen that velocity profiles similar to that of a coaxial jet [12] are obtained by installing deflectors inside the rectangular nozzle. Some interesting features can be observed in the  $x$ - $z$  plane. The jet spread for divergent deflectors is the smallest for these three jets at  $x/H = 6$ . In contrast, the jet spread for convergent deflectors is the largest for these three jets. These result in the direction opposite the mean streamwise velocity in the  $x$ - $y$  plane. **Figures 4(b)-(d)** show the profiles of mean streamwise velocity  $\bar{u}/U_0$  in the  $x$ - $y$  and  $x$ - $z$  cross sections for the three jets in order to compare the experimental results and the results of the numerical simulation. The experimental and numerical LES results show good agreement in the region from the nozzle exit at  $x/H = 0.1$  to the jet downstream region at  $x/H = 6$ . These results demonstrate that the LES simulation can reproduce the actual flow field.

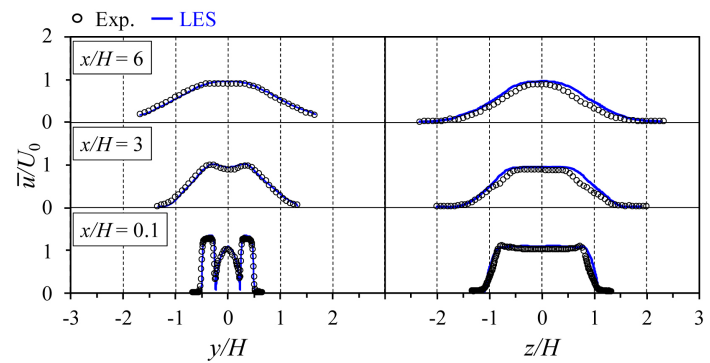
**Figure 5(a)** shows the profiles of the root mean square (RMS) values  $u'_{rms}/U_0$  of the fluctuating streamwise velocity components in the  $x$ - $y$  plane along the minor axis at  $z = 0$ , and the  $x$ - $z$  plane along the major axis side at  $y = 0$  to compare the three jets. In the  $x$ - $y$  plane, the velocity fluctuation for the jet with divergent deflectors near the center of the nozzle at  $x/H = 0.1$  is larger than that for the jet with convergent deflectors as a result of flow separation on the inner nozzle wall. At  $x/H = 6$ , the velocity fluctuation for the jet with divergent deflectors at the outer side of jet is larger than that for the jet with convergent deflectors.



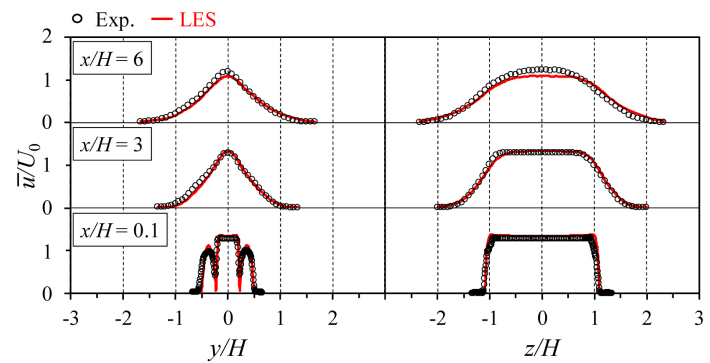
(a)



(b)



(c)



(d)

**Figure 4.** Profiles of mean streamwise velocity  $\bar{u}/U_0$  in the  $x$ - $y$  and  $x$ - $z$  planes. (a) Experiment; (b) No deflectors; (c) Divergent deflectors; (d) Convergent deflectors.

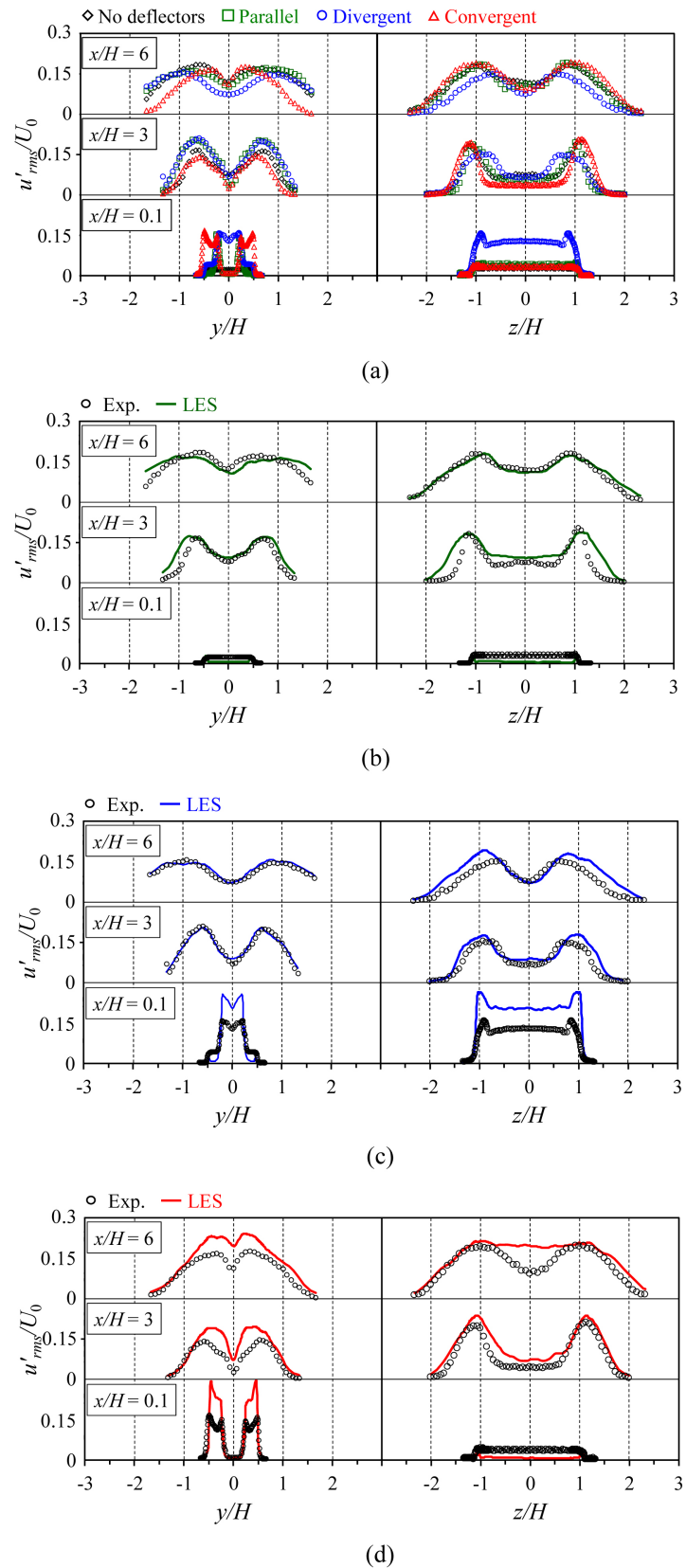


**Figure 5.** Profiles of the RMS velocity fluctuations  $u'_{rms}/U_0$  in the  $x$ - $y$  and  $x$ - $z$  planes. (a) Experiment; (b) No deflectors; (c) Divergent deflectors; (d) Convergent deflectors.

This phenomenon is related to the larger amount of spreading near the nozzle exit for the jet with divergent deflectors. For the jet with convergent deflectors, the velocity fluctuation near the centerline is smaller than those for the other jets. However, the turbulence intensity near the centerline at  $x/H \geq 5$  increases more than that for the jet with divergent deflectors. In addition, for the  $x$ - $z$  cross section, the velocity fluctuation at the nozzle exit is larger than that for the jet with convergent deflectors, and the growth rate for the velocity fluctuation near the centerline is low. **Figures 5(b)-(d)** show the profiles of the RMS values  $u'_{rms}/U_0$  for the fluctuating streamwise velocity components in the  $x$ - $y$  and  $x$ - $z$  cross sections for each jet to compare the experimental results and the results of the numerical simulation. For the jet with no deflectors, the LES results show fair agreement with the experimental results from near the nozzle exit at  $x/H = 0.1$  to downstream at  $x/H = 6$ . On the other hand, the agreement between the experimental and numerical results for the jets with divergent and convergent deflectors is poor in the upstream region. This difference may be caused that the transition flow from the flow of the relative low Reynolds number ( $Re = 9000$ ) to the turbulent flow cannot simulate with accuracy by the LES.

### 3.2. Mean Velocity and Turbulence Intensity along the Jet Centerline

**Figure 6** shows the mean streamwise velocity along the jet centerline in the experiment. The local centerline velocity  $\bar{u}$  is normalized by the bulk velocity  $U_0$  at the nozzle exit. The potential core length  $x_p$ , which is defined as the distance between the nozzle exit and the point at which the centerline velocity has decayed to 95% of its maximum value [13], is approximately  $7H$ ,  $8H$ ,  $0.5H$ , and  $10H$  for the jets with no deflectors, parallel plates ( $\bar{u}_{imax}/\bar{u}_{omax} = 1.0$ ), divergent deflectors ( $\bar{u}_{imax}/\bar{u}_{omax} = 0.8$ ), and convergent deflectors ( $\bar{u}_{imax}/\bar{u}_{omax} = 1.3$ ), respectively. In short, the length of the potential core also increases as the velocity ratio increases. This result agrees with previous experimental studies performed by Warda *et al.* [14] [15] and Mergheni *et al.* [16]. For divergent deflectors, the centerline velocity  $\bar{u}/U_0$  decreases from the vicinity of the nozzle exit and then

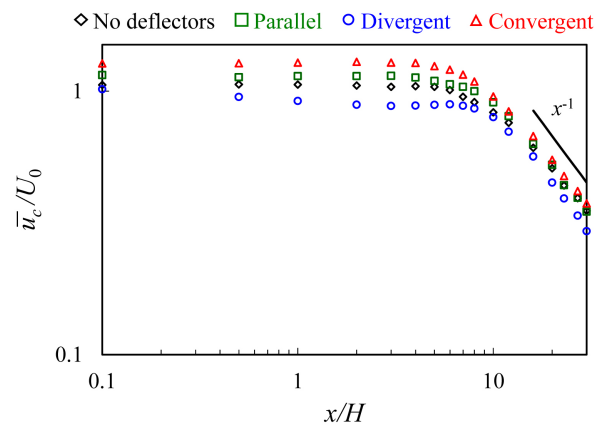


**Figure 6.** Profiles of mean streamwise velocity  $\bar{u}_c/U_0$  on the jet centerline.

has a minimum value at  $x/H = 3$ . This is similar to the results of Duroo and Whitelaw [17] and Buresti *et al.* [18] whereby the velocity decay ratio of the centerline velocity  $\bar{u}_c/U_0$  decreases immediately after the jet issues from the nozzle exit and the potential core length becomes short. In the far field at  $x/H > 10$ , the centerline velocity decreases at  $\bar{u}_c/U_0 \sim x^{-1}$  for all four jets, that is, this velocity decay ratio demonstrates behavior similar to that of a fully developed circular jet. Thus, this result shows that the rectangular jets with and without deflectors ultimately evolve into fully developed circular jets.

**Figure 7** shows the RMS value for the streamwise velocity fluctuations along the jet centerline in the experiment. For the jet with divergent deflectors, the velocity fluctuation at  $x/H < 3$  in the near field is larger than that for the other jets. However, the velocity fluctuation at  $x/H > 5$  is small in comparison with that for the other three jets. In the far field at  $x/H > 20$ , there is little difference between the velocity fluctuations for the four jets.

### 3.3. Growth of Jet Half-Velocity Width

**Figure 8** shows the growth of the jet half-velocity width obtained experimentally in the  $x$ - $y$  and  $x$ - $z$  planes. For the jet with no deflectors, the jet spreads rapidly along the minor axis in the  $x$ - $y$  plane and more slowly along the major axis in the  $x$ - $z$  plane. The axis-switching location  $x_{as}/H$ , where the length of  $y_{1/2}/H$  and  $z_{1/2}/H$  is reversed as a result of axis switching, is at  $x_{as}/H \approx 16$  (**Figure 8(a)**). In the case of the jet with parallel plates, axis switching occurs closer upstream ( $x_{as}/H \approx 8$ ) than the jet with no deflectors because the value of  $z_{1/2}/H$  does not change much for  $x/H < 8$  (**Figure 8(b)**). The jet with divergent deflectors spreads rapidly along the minor axis in the  $x$ - $y$  plane and shrinks along the major axis in the  $x$ - $z$  plane. As shown in **Figure 8(c)**, the value of  $z_{1/2}/H$  shows a decrease in the range of  $x/H$  from 0 to around 8 in  $x$  increases because of the relative low velocity area near the jet centerline, *i.e.* the ratio of the maximum velocity of the inner jet  $\bar{u}_{imax}$  to the outer jets  $\bar{u}_{omax}$  is  $\bar{u}_{imax}/\bar{u}_{omax} = 0.8$ . As a result, the jet shrinks the  $z$ -direction. Axis switching also occurs closer to the nozzle exit ( $x_{as}/H \approx 4$ )

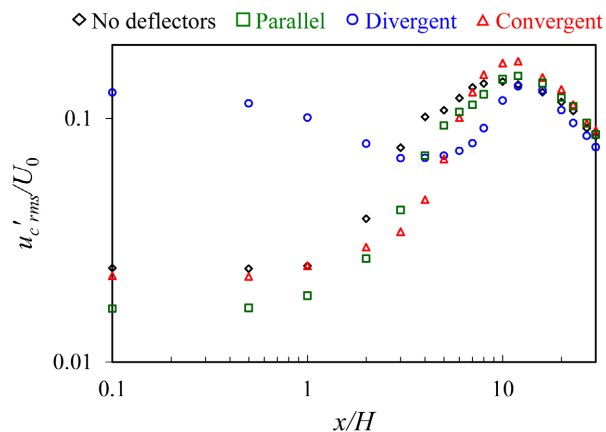


**Figure 7.** Profiles of the RMS streamwise velocity fluctuation  $u'_{rms}/U_0$  on the jet centerline.

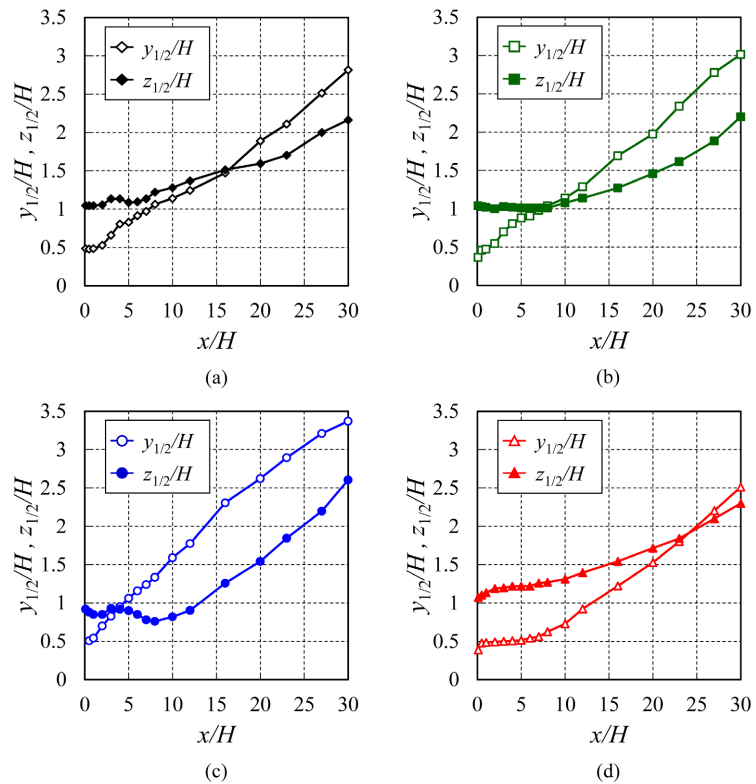


**Figure 8.** Variations in the jet half-velocity width in the  $x$ - $y$  and  $x$ - $z$  planes. (a) No deflectors; (b) Parallel plates; (c) Divergent deflectors; (d) Convergent deflectors.

than in the case of the jet with no deflectors. On the other hand, the jet with convergent deflectors spreads more slowly along the minor axis in the  $x$ - $y$  plane than the jet with no deflectors (**Figure 8(d)**). As a result, axis switching occurs farther downstream ( $x_{as}/H \approx 23$ ) than in the case of the jet with no deflectors. Therefore, the deflectors installed inside the rectangular nozzle influence the axis-switching location of the rectangular jet.

### 3.4. Equivalent Jet Half-Velocity Width Growth

**Figure 9** shows the equivalent jet spread, *i.e.*, the equivalent jet half-velocity width  $(y_{1/2} \times z_{1/2})^{0.5}/H$  [19], along the  $x$ -axis non-dimensionalized by the height of the nozzle. For comparison, the figure also reports the data of Kumar *et al.* [9] for a rectangular jet with an aspect ratio of 2 and Quinn [20] for a planar jet with an aspect ratio of 20. The equivalent jet spread signifies the overall spread of the jet along the  $x$ -axis based on the given exit conditions. The equivalent jet spread for the nozzle with no deflectors is greater than that for the nozzle with divergent deflectors and less than that for the nozzle with the convergent deflectors. The jet spread along the minor axis is made dominant by the introduction of deflectors inside the nozzle. Although the jet half-velocity widths  $y_{1/2}/H$  and  $z_{1/2}/H$  in each plane shown in **Figure 8** exhibit nonlinear variation with  $x/H$ , the equivalent jet half-velocity width  $(y_{1/2} \times z_{1/2})^{0.5}/H$  varies linearly with  $x$  for  $x/H > 10$ . The spreading rate for the present jets shows close agreement with the data

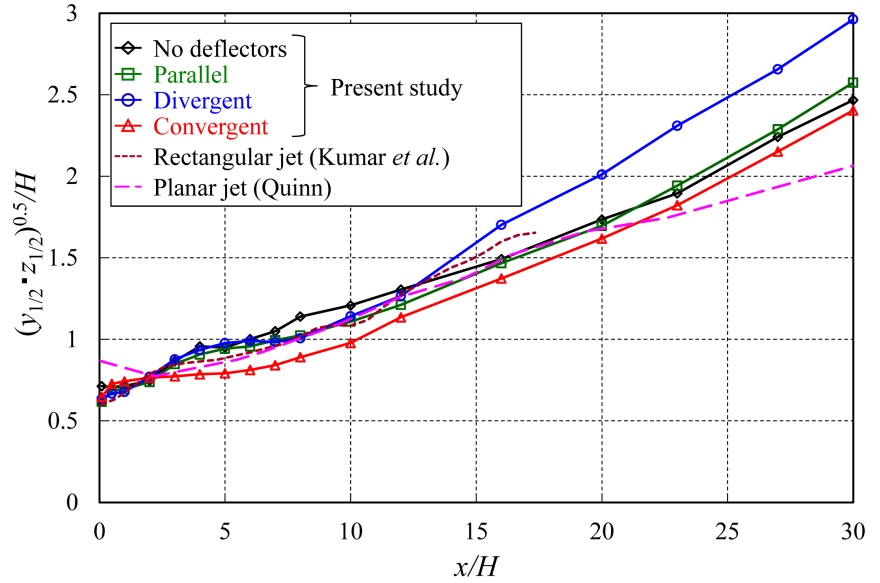


**Figure 9.** Equivalent jet half-velocity width.

**Table 1.** Spreading rates and geometric vertical origins obtained by fitting experimental data with Equation (1).

| Jet                                    | $B/H$ | $K_s$  | $C_s$ | Range               |
|--|-------|--------|-------|---------------------|
| No deflectors                          |       | 0.0625 | -8.5  |                     |
| Parallel plates                        | 2.17  | 0.0725 | -4.5  |                     |
| Divergent deflectors                   |       | 0.0913 | -2.3  | $10 < x/H < 30$     |
| Convergent deflectors                  |       | 0.0696 | -3.9  |                     |
| Rectangular jet (Kumar <i>et al.</i> ) | 2     | 0.0714 | -6    | $6.67 < x/H < 17.3$ |
| Planar jet (Quinn)                     | 20    | 0.0439 | -17.4 | $12 < x/H < 30$     |

of Kumar *et al.* [9] and Quinn [20]. Therefore, the jet spread data in **Figure 9** were fitted by linear regression analysis using the function

$$\frac{(y_{1/2} \cdot z_{1/2})^{0.5}}{H} = K_s \left( \frac{x}{H} + C_s \right) \tag{1}$$

where  $K_s$  is the spreading rate, and  $C_s$  is the geometric virtual origin. The values of these parameters obtained in the fitting are given in **Table 1** for each of the cases plotted in **Figure 9**. There is a difference between the spreading rates  $K_s$  for the 2.17:1 and 20:1 rectangular jets. In general, rectangular jets with small aspect ratios generate three-dimensional flow fields, whereas those with large aspect ratios generate two-dimensional flow fields. Note that the spreading rate  $K_s$  for the jet with divergent deflectors is larger than those for the other jets.

### 3.5. Deformation of Jet Outline

**Figure 10** shows the contours of mean streamwise velocity for the three jets obtained experimentally in the quarters of the  $y$ - $z$  plane at  $x/H = 1, 4, 10,$  and  $16$ .

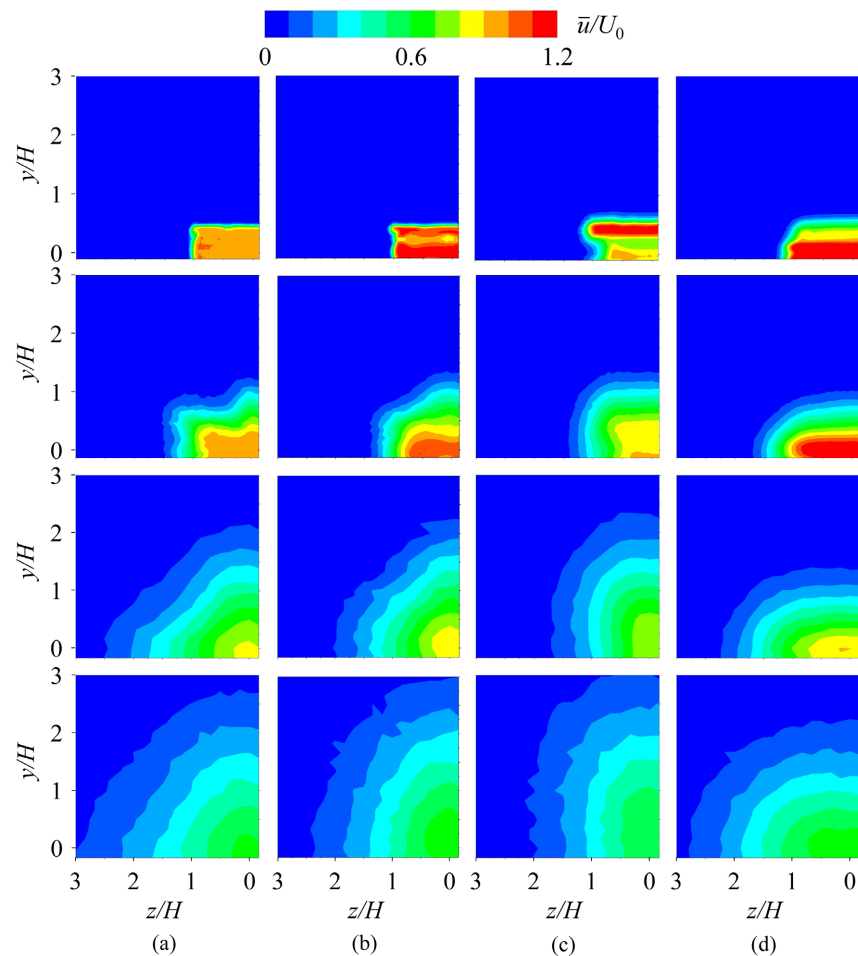


**Figure 10.** Mean streamwise velocity contour plots in the quarters of  $y$ - $z$  cross section at  $x/H = 1, 4, 10$  and  $16$ . (a) No deflectors; (b) Parallel plates; (c) Divergent deflectors; (d) Convergent deflectors.

These measurements of grid points were carried out for a step size of  $\Delta y = \Delta z = 1.0$  mm for  $x/H = 1$ ,  $\Delta y = \Delta z = 2.0$  mm for  $x/H = 4$ , and  $\Delta y = \Delta z = 5.0$  mm for  $x/H = 10$  and  $16$ , respectively. The contour interval is  $0.1 U_0$ . As shown in **Figure 10(a)**, immediately downstream of the nozzle exit, *i.e.*,  $x/H = 1$ , the rectangular jet with no deflectors retains the original shape of the rectangular nozzle, and the jet has a thin shear layer at the circumference of the nozzle. The jet deformation begins at the nozzle corners because of the nonuniform velocity induction (seen as an outward bump in the contours). As a result, the ambient fluid was brought in toward the jet centerline along the major axis side while the jet fluid was ejected along the minor axis side. Further downstream, the shear layer becomes thick and the shape of the jet changed as there was high growth along the minor axis side. The outline of the jet at  $x/H = 16$  changes from rectangular to diamond-shaped, accompanied by axis switching. In the case of the jet with parallel plates (**Figure 10(b)**), the velocity defect occurs due to the wakes of the parallel plates at  $x/H = 1$ . However, the jet maintains a rectangular shape, as is the case for a jet with no deflectors. The axis switching occurred for  $x/H > 10$ . In the

case of the jet with divergent deflectors (**Figure 10(c)**), at  $x/H = 1$ , the velocity in the outer mixing region is larger than that in the inner mixing region. The thickness of the shear layer at the long side of the rectangular nozzle at  $x/H = 4$  is thinner than that at the short side. The jet outline is extended by high growth along the minor axis side for  $x/H > 4$ . As a result, the jet shape changes from a lateral rectangle to a vertical ellipse. On the other hand, as shown in **Figure 10(d)**, the jet with convergent deflectors has a thin shear layer at the short side of the rectangular nozzle at  $x/H = 1$ , as compared with the long side. The jet extends more rapidly along the major axis side than along the minor axis side. Consequently, the jet outline at  $x/H = 16$  roughly maintains the rectangular shape of the nozzle exit without axis switching occurring.

### 3.6. Instantaneous Vorticity Contours and Vortex Shedding Frequency

**Figure 11** shows instantaneous vorticity contours in the  $x$ - $y$  plane along the minor axis side at  $z = 0$  for the three jets obtained by the large-eddy simulation. Vortex roll-up is observed in the shear layers at the nozzle exit, and vortices of opposite signs are positioned symmetrically about the jet centerline at  $x/H \approx 1.2$  for the jet with no deflectors (as shown in **Figure 11(a)**). For the case of the jet

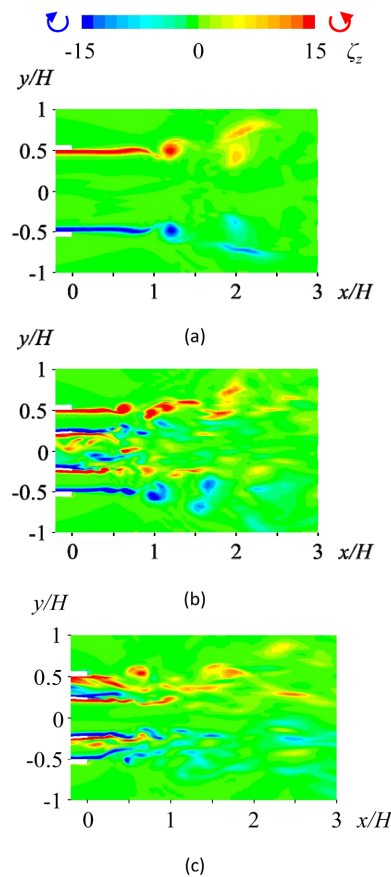


**Figure 11.** Instantaneous  $z$ -vorticity contours of rectangular jets in the  $x$ - $y$  plane. (a) No deflectors; (b) Divergent deflectors; (c) Convergent deflectors.

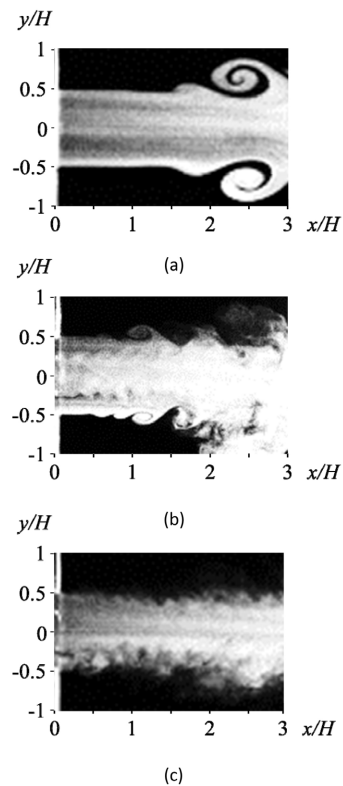


**Figure 12.** Instantaneous images of rectangular jets in the  $x$ - $y$  plane. (a) No deflectors; (b) Divergent deflectors; (c) Convergent deflectors.

with divergent deflectors (**Figure 11(b)**), vertex roll-up is observed in the outer shear layers at  $(x/H, y/H) \approx (0.5, \pm 0.5)$ . In the inner shear layer, the separated vortices on the inner wall surface of the deflectors interact with the vortices on the outer surfaces of the deflectors. As a result, the velocity fluctuation near the nozzle exit of the jet with divergent deflectors increased, as shown in **Figure 5(c)**. In the case of the jet with convergent deflectors (**Figure 11(c)**), the periodic vortex shedding in the outer shear layers is suppressed, unlike in the jets with no deflectors or divergent deflectors. This phenomenon affects the separated flow generated on the outer surface of the deflectors in the rectangular nozzle, and then the mixing with the ambient fluid is suppressed. As a result, the rectangular jet does not spread along the  $y$ -direction, as shown in **Figure 10(d)**. The flow structures can be changed by adjusting the deflectors. These results are consistent with the instantaneous flow visualization images qualitatively, as shown in **Figure 12**. For the jet with no deflectors, the periodic vortical structure, *i.e.*, the vortex ring in the  $x$ - $y$  cross section is arranged symmetrically with respect to the  $x$ -axis and changes to a small-scale vortical structure in the downstream. On the other hand, for the jets with divergent and convergent deflectors, the large-scale vortical structures are not clear in the shear layers.

**Figure 13** shows the power spectra of the streamwise fluctuating velocity in the outer ( $x/H = 0.5, y/H = 0.5, z/H = 0$ ) and inner ( $x/H = 0.22, y/H = 0.22, z/H = 0$ ) mixing regions obtained by the numerical simulation. For the jet with no

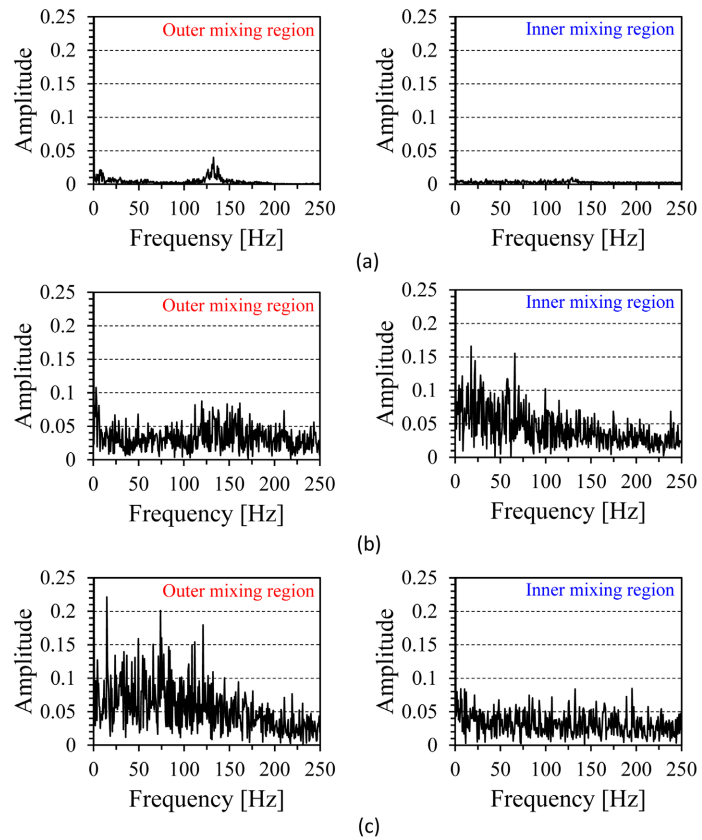


**Figure 13.** Power spectra of the velocity fluctuations of rectangular jets in the outer ( $x/H = 0.5$ ,  $y/H = 0.5$ ,  $z/H = 0$ ) and inner ( $x/H = 0.22$ ,  $y/H = 0.22$ ,  $z/H = 0$ ) mixing regions obtained by numerical simulation. (a) No deflectors; (b) Divergent deflectors; (c) Convergent deflectors.

deflectors (**Figure 13(a)**),  $f_p \approx 132$  Hz for the predominant spectrum peak in outer mixing region. In the experiment, the peak frequency of the streamwise fluctuating velocity in the outer mixing region ( $x/H = 1$  and  $2$ ) was  $f_p \approx 118$  Hz. The Strouhal numbers  $St_H (=f_p H / U_0)$  for these peak frequencies in the LES and experiment are 0.88 and 0.79, respectively. Thus, the peak frequency obtained from the LES agrees approximately with the experimental value in the outer mixing region. For the jet with divergent deflectors (**Figure 13(b)**), a peak frequency of  $f_p \approx 18$  Hz is observed in the inner mixing region. Three clear peaks in the power spectra at 15, 74, and 121 Hz are observed in the outer mixing region near the nozzle of the jet with convergent deflectors (**Figure 13(c)**). The Strouhal numbers  $St_H$  for these frequencies are 0.1, 0.493, and 0.806, respectively.

### 3.7. Instantaneous Three-Dimensional Vortical Structures

**Figure 14** shows instantaneous three-dimensional vortical structures for the three jets based on the second invariant isosurfaces of the velocity gradient tensor  $Q$ . In the case of the jet with no deflectors (**Figure 14(a)**), the vortex rings are generated and maintained periodically from the nozzle exit until  $x/H \approx 3$ . The vortex ring collapses, and vortical structures, such as hairpin vortices, are

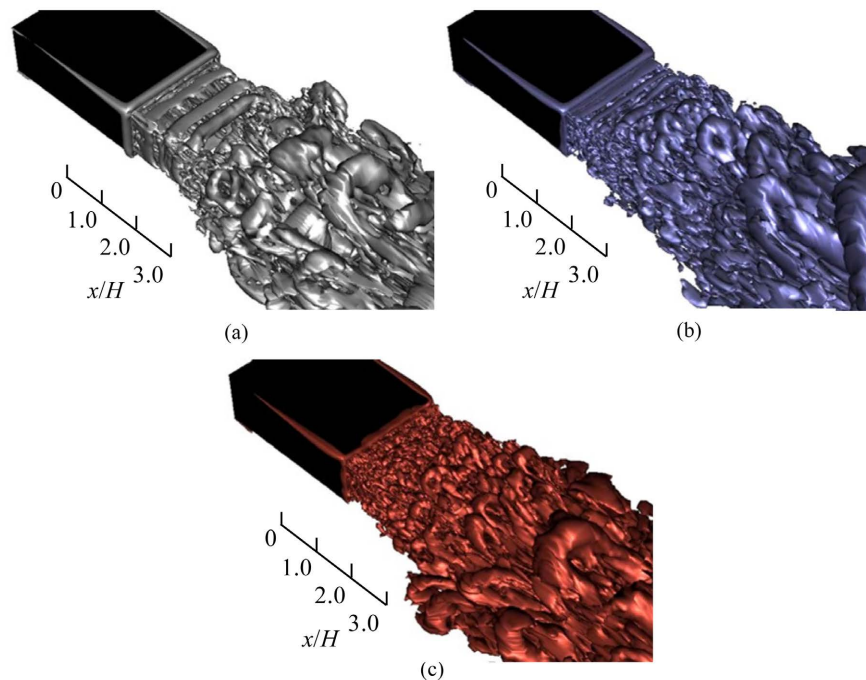


**Figure 14.** Second invariant isosurface of the velocity gradient tensor  $Q$  for the rectangular jets. (a) No deflectors; (b) Divergent deflectors; (c) Convergent deflectors.

generated in the downstream region. In the case of the jet with divergent deflectors (**Figure 14(b)**), intermittent shedding of the vortex ring is observed, and its scale is smaller than that for the rectangular jet with no deflectors. In the downstream region, a large-scale vortical structure develops. In the case of the rectangular jet with convergent deflectors (**Figure 14(c)**), a vortical structure also develops in the same manner as for the rectangular jet with divergent deflectors. These vortical structures agree with the instantaneous images of rectangular jets in the  $x$ - $y$  plane qualitatively, as shown in **Figure 12**.

#### 4. Conclusions

The influence of the angle between two plates inside the nozzle, *i.e.* divergent and convergent deflectors, on the flow characteristics and vortical structures of a rectangular jet with an aspect ratio of  $AR = 2.17$  was investigated experimentally and through large-eddy simulation. The following conclusions were reached in the present study.

1) The mean velocity distributions obtained by numerical simulations using LES are in good agreement with the experimental results. The turbulence intensity distribution obtained by LES is in approximate agreement with the experimental results. LES can accurately simulate the three-dimensional flow structures of rectangular jets with deflectors.

2) In the case of the jet with divergent deflectors, a small-scale vortical structure is generated in the outer shear layer, and the turbulence intensity in the inner mixing region is high because of the separated flow on the deflector walls. As

a result, the equivalent spread of the jet is higher and axis switching occurred closer to the nozzle exit than in the case of the jet with no deflectors.

3) In the case of the jet with convergent deflectors, a vortex ring was not observed in the outer shear layer, and the turbulence intensity in the outer mixing region was high because of the separated flow on the deflector walls. As a result, the equivalent spread of the jet is lower and axis switching occurred farther from the nozzle exit than in the case of the jet with no deflectors. Therefore, the rectangular jet spread can be controlled by the slant angle of deflectors installed inside the rectangular nozzle.

### Acknowledgements

The present study was supported by a JSPS Grant-in-Aid for Scientific Research (Grant Number 19K04166). The authors are thankful to Mr. Kuratani for his help in conducting the experiment.

### Conflicts of Interest

The authors declare no conflicts of interest regarding the publication of this paper.

### References

- [1] Aleyasin, S.S., Tachie, M.F. and Koupriyanov, M. (2017) PIV Measurements in the Near and Intermediate Field Regions of Jets Issuing from Eight Different Nozzle Geometries. *Flow, Turbulence and Combustion*, **99**, 329-351. <https://doi.org/10.1007/s10494-017-9820-3>
- [2] Mi, J. and Nathan, G.J. (2010) Statistical Properties of Turbulent Free Jets Issuing from Nine Differently-Shaped Nozzles. *Flow, Turbulence and Combustion*, **84**, 583-606. <https://doi.org/10.1007/s10494-009-9240-0>
- [3] Schadow, K.C., Gutmark, E., Parr, D.M. and Wilson, K.J. (2004) Selective Control of Flow Coherence in Triangular Jets. *Experiments in Fluids*, **6**, 129-135. <https://doi.org/10.1007/BF00196464>
- [4] Ghasemi, A., Roussinova, V., Balachandar, R. and Barron, R.M. (2015) Reynolds Number Effects in the Near-Field of a Turbulent Square Jet. *Experimental Thermal and Fluid Science*, **61**, 249-258. <https://doi.org/10.1016/j.expthermflusci.2014.10.025>
- [5] Sfier, A.A. (1979) Investigation of Three-Dimensional Turbulent Rectangular Jets. *AIAA Journal*, **17**, 1055-1060. <https://doi.org/10.2514/3.61277>
- [6] Quinn, W.R. (1992) Turbulent Free Jet Flows Issuing from Sharp-Edged Rectangular Slots: The Influence of Slot Aspect Ratio. *Experimental Thermal and Fluid Science*, **5**, 203-215. [https://doi.org/10.1016/0894-1777\(92\)90007-R](https://doi.org/10.1016/0894-1777(92)90007-R)
- [7] Ho, C. and Gutmark, E. (1987) Vortex Induction and Mass Entrainment in a Small-Aspect-Ratio Elliptic Jet. *Journal of Fluid Mechanics*, **179**, 383-405. <https://doi.org/10.1017/S0022112087001587>
- [8] Fujita, S., Harima, T. and Osaka, H. (2009) Turbulent Jets Issuing from the Rectangular Nozzle with a Rectangular Notch at the Midspan. *Fluid Structure Interaction V*, **105**, 61-70. <https://doi.org/10.2495/FSI090061>
- [9] Kumar, P.A., Verma, S.B. and Elangovan, S. (2011) Study of Jets from Rectangular Nozzles with Square Grooves. *Journal of Fluid Mechanics*, **115**, 187-196.

- <https://doi.org/10.1017/S0001924000005583>
- [10] Verma, S.B., Sudhakar, S. and Venkatakrishnan, L. (2010) Experimental Study on Jet Issuing from an Elliptic Nozzle with Cylindrical Tabs. *Journal of Turbulence*, **11**, Article No. N20. <https://doi.org/10.1080/14685248.2010.490221>
- [11] Hinomoto, W., Kiwata, T., Usuzawa, T., Kimura, S. and Komatsu, T. (2012) Flow Characteristics of a Plane Jets with Deflectors inside a Nozzle. *Proceedings of the 8th KSME-JSME Thermal and Fluids Engineering Conference (TFEC8)*, Songdo, 18-21 March 2012, 1-4.
- [12] Kiwata, T., Usuzawa, T., Komatsu, N., Kimura, S. and Oshkai, P. (2011) Flow Structure of a Coaxial Circular Jet with Axisymmetric and Helical Instability Modes. *Journal of Fluid Science and Technology*, **6**, 437-452. <https://doi.org/10.1299/jfst.6.437>
- [13] Livingood, J.N.B. and Hrycak, P. (1973) Impingement Heat Transfer from Turbulent Air Stream Jets to Flat Plate: A Literature Survey. NASA Technical Memorandum.
- [14] Warda, H.A., Kassab, S.Z., Elshorbagy, K.A. and Elsaadawy, E.A. (1999) An Experimental Investigation of the Near-Field Region of a Free Turbulent Coaxial Jet using LDA. *Flow Measurement and Instrumentation*, **10**, 15-26. [https://doi.org/10.1016/S0955-5986\(98\)00041-7](https://doi.org/10.1016/S0955-5986(98)00041-7)
- [15] Warda, H.A., Kassab, S.Z., Elshorbagy, K.A. and Elsaadawy, E.A. (1999) Influence of the Magnitude of the Two Initial Velocities on the Flow Field of a Coaxial Turbulent Jet. *Flow Measurement and Instrumentation*, **12**, 29-35. [https://doi.org/10.1016/S0955-5986\(00\)00037-6](https://doi.org/10.1016/S0955-5986(00)00037-6)
- [16] Mergheni, M.A., Boushaki, T., Sautet, J.C., Godard, G., Ticha, H.B. and Nasrallah, S.B. (2008) Effects of Different Mean Velocity Ratios on Dynamics Characteristics of a Coaxial Jet, *Thermal Science*, **12**, 49-58. <https://doi.org/10.2298/TSCI0802049M>
- [17] Duraó, D. and Whitelaw, J.H. (1973) Turbulent Mixing in the Developing Region of Coaxial Jets, *Journal of Fluids Engineering*, **95**, 467-473. <https://doi.org/10.2298/TSCI0802049M>
- [18] Buresti, G., Talamelli, A. and Petagna, P. (1994) Experimental Characterization of the Velocity Field of a Coaxial Jet Configuration. *Experimental Thermal and Fluid Science*, **9**, 135-146. [https://doi.org/10.1016/0894-1777\(94\)90106-6](https://doi.org/10.1016/0894-1777(94)90106-6)
- [19] Srinivasan, K. and Rathakrishnan, E. (2000) Studies on Polygonal Slot Jets. *AIAA Journal*, **38**, 1985-1987. <https://doi.org/10.2514/2.855>
- [20] Quinn, W.R. (1994) Development of a Large-Aspect-Ratio Rectangular Turbulent Free Jet. *AIAA Journal*, **32**, 547-554. <https://doi.org/10.2514/3.12020>

## Nomenclature

- $AR$  = aspect ratio of nozzle  
 $B$  = width of nozzle  
 $C_s$  = geometric virtual origin  
 $f_p$  = peak frequency  
 $H$  = height of nozzle  
 $H_i$  = distance between deflectors  
 $K_s$  = spreading rate  
 $L$  = length of deflector  
 $p$  = pressure outlet  
 $Q$  = second invariant isosurface of velocity gradient tensor  
 $Re_H$  = Reynolds number ( $= U_0 H / \nu$ )  
 $St_H$  = Strouhal number ( $= f_p H / U_0$ )  
 $t$  = thickness of deflector  
 $U$  = Inlet velocity  
 $U_0$  = bulk velocity at center of nozzle exit ( $z = 0$ )  
 $\bar{u}_{0c}$  = mean centerline  $x$ -component of velocity at nozzle exit ( $x/H = 0.1$ )  
 $\bar{u}_c$  = mean centerline  $x$ -component of velocity  
 $\bar{u}_{imax}$  = maximum velocity of inner jet at nozzle exit ( $x/H = 0.1$ )  
 $\bar{u}_{omax}$  = maximum velocity of outer jet at nozzle exit ( $x/H = 0.1$ )  
 $u'_{rms}$  = RMS value of  $x$ -component of velocity fluctuation  
 $u'_{crms}$  = RMS value of centerline  $x$ -component of velocity fluctuation  
 $\bar{u}$  = mean  $x$ -component of velocity  
 $x$  =  $x$ -coordinate  
 $x_{as}$  = axis-switching location  
 $x_p$  = potential core length  
 $y$  =  $y$ -coordinate  
 $y_{1/2}$  = jet half-velocity width in  $x$ - $y$  cross section  
 $z$  =  $z$ -coordinate  
 $z_{1/2}$  = jet half-velocity width in  $x$ - $z$  cross section  
 $a$  = angle between the parallel and deflector plates  
 $\nu$  = kinematic viscosity of air  
 $\zeta_z$  =  $z$ -vorticity